electronics

MDPI

Article

A Hybrid Antenna with Equal Beamwidth in Two Frequency Bands for Radar Applications

Ning Zhang [1,2], Changjiang Deng [1,*] and Houjun Sun [1]

[1] Beijing Key Laboratory of Millimeter Wave and Terahertz Technology, The School of Information and Electronics, Beijing Institute of Technology, Beijing 100081, China; 3120160340@bit.edu.cn (N.Z.); sunhoujun@bit.edu.cn (H.S.)
[2] Beijing Institute of Space Long March Vehicle, Beijing 100076, China
* Correspondence: dengcj11@bit.edu.cn; Tel.: +86-010-6891-5628

Abstract: This paper presents a novel hybrid antenna with equal beamwidth in two frequency bands for short-range radar applications. The proposed design consists of a 2 × 2 patch array and a SIW-fed dielectric rod antenna. The two kinds of radiators are responsible for the 5.8 GHz and 24 GHz ISM bands, respectively. Pencil beams are obtained in both lower and upper bands. The beamwidth generated by the dielectric rod can be flexibly tuned to coincide with that of the patch array. Magneto-electric (ME) dipole, composed of a slot and two parasitic monopoles, is constructed to replace the conventional 3-D waveguide feeder, which can excite the dielectric rod effectively. The complementary structure is helpful to obtain a pencil beam. The 2 × 2 patch array has the size of 70 × 70 mm^2 and is fed by a four-way power divider. Due to no overlapping radiating aperture, the two radiators can work independently with high port isolation. The measured peak gain in the two bands is 12.5 dBi and 12.7 dBi. The measured 3-dB beamwidth at 5.8 GHz and 24 GHz is 42° and 39° in *x*-*z* plane, and 43° and 42° in the *y*-*z* plane. The proposed antenna features a small beamwidth difference in two frequency bands, thus being attractive for dual-band radar systems.

Keywords: dual-band antennas; dielectric rod antennas; patch antennas; radar antennas

Citation: Zhang, N.; Deng, C.; Sun, H. A Hybrid Antenna with Equal Beamwidth in Two Frequency Bands for Radar Applications. *Electronics* **2021**, *10*, 3000. https://doi.org/10.3390/electronics10233000

Academic Editor: Dimitra I. Kaklamani

Received: 11 November 2021
Accepted: 29 November 2021
Published: 2 December 2021

1. Introduction

Radar technology plays an important role in modern wireless systems. Nowadays, dual-band radar receives growing interest since it can provide two independent frequency channels regarding the detected object. The enhanced spectrum information is beneficial to improve the accuracy and robustness of the radar system. In recent decades, dual-band radars have been applied in various applications, such as remote sensing and autonomous driving [1–4].

As one of the key components in a dual-band radar system, dual-band antennas have been intensively researched [5–7]. According to the radiation gain level, the related dual-band antennas are categorized into three types, namely high gain, medium gain, and low gain antennas. Parabolic reflector and reflectarray are widely used in high gain design [8–10]. In medium-gain antenna design, the available radiators are rich, including horn, dielectric rod antenna, patch array, and their combinations [11–19]. As for low gain antennas, dual-band operation is one of the most popular topics. Many dual-band antennas based on patch, slot, dipole, and monopole have been proposed [20–27]. However, to the best of the authors' knowledge, almost all the designs did not concern the beamwidth relationship in the two bands. The beamwidth in the upper band is usually narrower owing to a shorter wavelength. This behavior may cause serious problems in some radar applications. Figure 1 show one possible application of dual-band radar, where the radar emits two beams at two different frequencies. In Figure 1a, the illumination areas of the two beams are different since the beamwidth in the two bands is not equal. It means that the information obtained from the reflected waves may be different at the two frequencies. In

Figure 1b, identical illumination areas are achieved in the two bands because the two beams have equal beamwidth. This property is especially useful for the detection of atmospheric particles, such as clouds, snow, and rain. Considering that the particles are separately distributed, identical beamwidth can guarantee the same illuminating volume of particles in two bands.

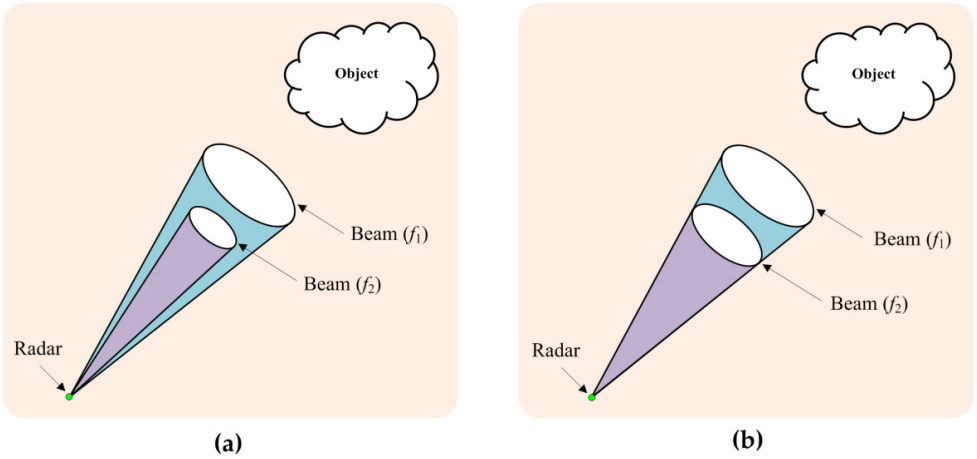

Figure 1. Dual-band radar emitting two independent beams: (**a**) Unequal beamwidth in two frequency bands; (**b**) Equal beamwdith in two frequency bands. Atmospheric particles, such as clouds, snow, and rain, are the typical detected objects.

In this paper, a dual-band antenna that has medium gain and equal beamwidth is presented for radar applications. The hybrid antenna combines a patch array and a dielectric rod antenna. The two kinds of radiators generate resonances in the lower and upper bands, respectively. The beamwidth of the dielectric rod antenna is changed to coincide with that of the patch array. However, a bulky 3-D waveguide is usually needed to feed the dielectric rod [28,29]. This makes the antenna difficult to integrate with a planar circuit. A planar feed network has been proposed to replace 3-D waveguides [30–34]. For example, in ref. [30], a planar waveguide is fabricated by stacking multiple layers. In ref. [32], a single-layer substrate integrated waveguide (SIW) feeder is used to excite the dielectric rod. However, the main beam is towards the end-fire direction, not towards the broadside direction. In the proposed antenna, a novel planar magneto-electric (ME) dipole is designed to excite a dielectric rod. This has the merits of simple structure and symmetrical radiation pattern. In addition, the low mutual coupling is needed in many wireless systems [35–37]. Thanks to no overlapping radiating aperture, the proposed antenna can achieve high port isolation in the two bands.

There are two innovations in this work. Firstly, the concept of equal beamwidth in two frequency bands is proposed for the first time. This is helpful to improve the detection accuracy of radar. Secondly, the dielectric rod is fed by SIW rather than a bulky 3-D waveguide. An ME dipole is constructed to amend the distortion of the radiation pattern caused by the SIW feed. The feed structure is easy to integrate with a planar circuit.

2. Antenna Design Methodology

2.1. Antenna Geometery

To obtain medium gain (i.e., 10–20 dBi) performance in two frequency bands, a hybrid antenna structure is proposed. As shown in Figure 2, it combines a patch array and a dielectric rod antenna. The patch array and its feed network are printed on the top layer of the upper substrate. The dielectric rod is located at the center and is fed by a SIW feed network. The SIW structure is fabricated on the lower substrate. A slot is etched on the ground plane to couple energy from the SIW feeder to the dielectric rod. Two parasitic metallic pins are placed in the upper substrate, which is beneath the rod. A

tapered transition is printed at the bottom layer of the lower substrate to transform the input impedance of the SIW feeder to 50 Ω. The detailed dimensions are listed in Table 1.

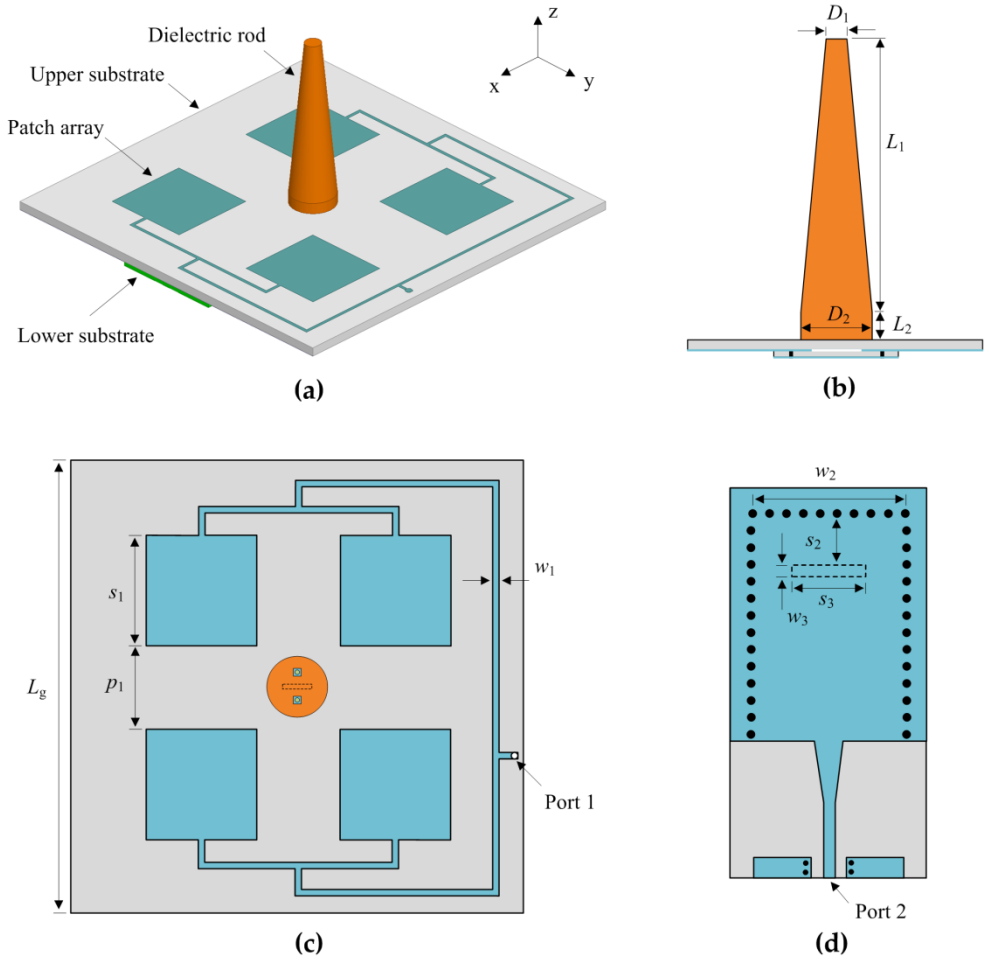

Figure 2. Geometry and dimensions of the proposed hybrid dual-band antenna: (**a**) 3-D view; (**b**) Side view; (**c**) Dimensions of the patch array on the top layer; (**d**) Dimensions of the SIW feed on the bottom layer.

Table 1. Detailed dimensions of the antenna (unit: mm).

Parameter	Value	Parameter	Value	Parameter	Value
D_1	3	L_2	2	w_2	11
D_2	8	p_1	16	s_2	3
L_1	29	w_1	0.6	w_3	0.5

The patch array is responsible for the lower band. The typical gain of a 2 × 2 patch array is roughly 13 dBi. Higher gain can be obtained by using a 3 × 3 or 4 × 4 patch array. The dielectric rod is responsible for the upper band. As we know, the typical gain of dielectric rod varies from 10 dBi to 20 dBi. The gain increases with the increase of the rod's length. It provides a simple but flexible way to change the beamwidth. That is why a dielectric rod radiator is adopted in the proposed design.

2.2. Operating Principle of the Dielectric Rod Antenna

A dielectric rod antenna is used to generate a pencil beam in the upper band. This kind of radiator has a small transversal size and high gain. In addition, the gain is mainly decided by the longitudinal length of the rod. These properties are useful in gaining

adjustment. Nevertheless, as shown in Figure 3a, the rod usually needs to be inserted into a waveguide, and there is a tapered transition at the bottom of the rod.

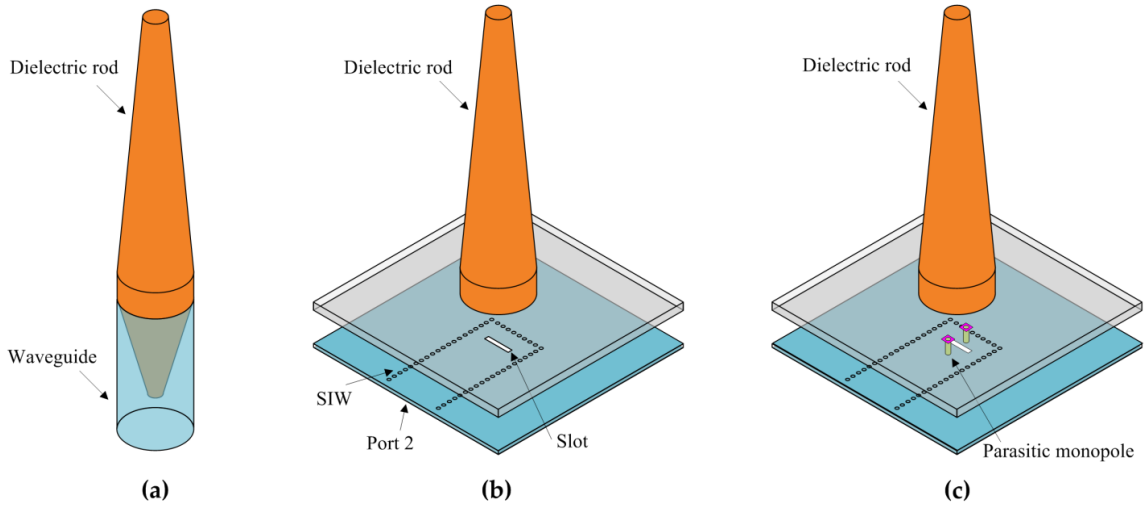

Figure 3. Design evolution of the feeding network for dielectric rod antenna: (**a**) Using a conventional 3-D waveguide feed; (**b**) Using a planar SIW feed; (**c**) Using a planar SIW feed with a pair of parasitic monopoles.

In order to get rid of the bulky feed and the tapered transition, the conventional 3-D waveguide is replaced by planar SIW in this design. As shown in Figure 3b, the dielectric rod is placed above the SIW feeder. No tapered transition is needed at the bottom of the rod. The dielectric rod is made of low-cost Teflon (ε_r = 2.1, tan δ = 0.001). A slot is etched on the top surface of the SIW, where RT/duroid 5880 substrates with a thickness of 0.508 mm are used. There is a thick substrate layer between the dielectric rod and the slot. It refers to the substrate in patch array design. The initial size of the ground plane is 40 × 40 mm^2. This value will be adjusted when assembling with the patch array.

The center frequency of the dielectric rod is designated for the 24 GHz ISM band. Figure 4a show the radiation patterns of the rod fed by the SIW directly. It is shown that the patterns in the two principal planes are distorted. The main beam is not pencil, and the beamwidth in the two planes is also not equal. The reason is that there is no tapered transition between the rod radiator and the SIW feed. Large discontinuity causes the turbulence of the beam.

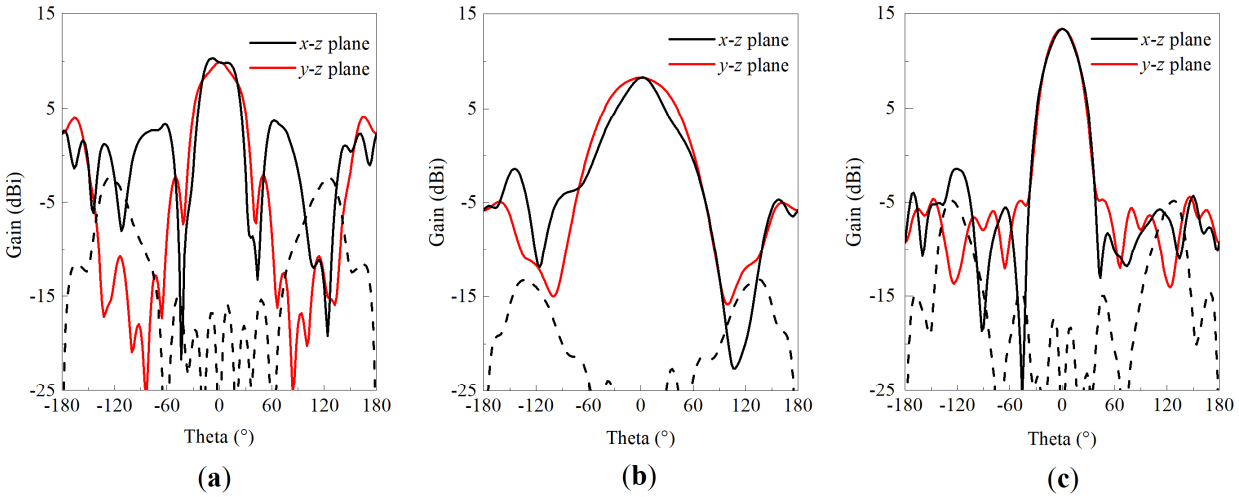

Figure 4. Radiation patterns at 24 GHz: (**a**) Dielectric rod antenna using a planar SIW feed; (**b**) Slot and monopole feeder without dielectric rod; (**c**) Dielectric rod antenna using a SIW feed with a pair of parasitic monopoles.

The feed network is modified to amend the distortion of the radiation pattern. As shown in Figure 3c, a pair of parasitic metallic pins are inserted in the upper substrate. The two pins are located at the mid perpendicular line of the slot and have a distance of 2.8 mm. The height of the pins is the thickness of the upper substrate and is 1.575 mm. This value is roughly $\lambda/4$ at 24 GHz when taking the dielectric constant into consideration. Therefore, the two pins serve as two parasitic $\lambda/4$ monopoles, which can also radiate energy effectively.

Figure 4b show the radiation patterns of the slot and monopoles before adding the dielectric rod. It is seen that a pencil beam can be generated when only the slot and monopole feeder is excited. The beamwidth in the two principal planes has a small difference, which is caused by the fact that the effective permittivity for the monopoles is slightly decreased if the dielectric rod is moved away from the top of the monopoles. The peak gain of the slot and monopoles is about 8.3 dBi.

The simulated radiation patterns with parasitic monopoles and dielectric rods are shown in Figure 4c. The main beamwidth in the *x*-*z* and *y*-*z* planes agrees well. The peak gain is 13.4 dBi in the zenith direction, and the 3-dB beamwidth in the *x*-*z* and *y*-*z* planes is 34.7° and 35.8°. The two values are almost equal, indicating that a pencil beam is obtained. Therefore, the distortion of the radiation patterns can be well amended.

The operating principle of the feed network is further analyzed to explain the amendment of the radiation patterns. As depicted in Figure 5, the feed network is considered to be a ME dipole. On the one hand, the length of the slot is about half-wavelength. The slot serves as a magnetic dipole. The direction of magnetic current J_M is transversal with respect to the slot. On the other hand, the length of the parasitic monopoles is about quarter-wavelength. The currents on the two monopoles are out of phase since the monopoles are located at the two sides of the slot. Therefore, the two monopoles serve as an electric dipole. The direction of equivalent current J_E is also transversal with respect to the slot. The ME dipole is constructed based on the slot and the monopoles. As we know, the ME dipole has symmetrical radiation patterns in E- and H-planes [38]. The pencil beam remains unchanged when a dielectric rod is placed above the ME dipole because the dielectric rod can also emit a pencil beam.

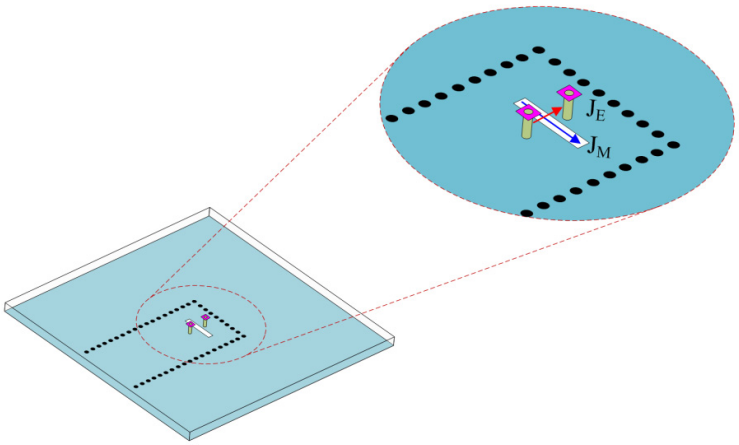

Figure 5. Operating principle of the SIW feed network with equivalent ME dipole.

Figure 6 show the surface currents distribution on the ground plane. The currents are concentrated at the two ends of the slots and around the two monopoles. The square contour of the current intensity can be observed at the center area. The current distribution further indicates that an equivalent ME dipole has been constructed.

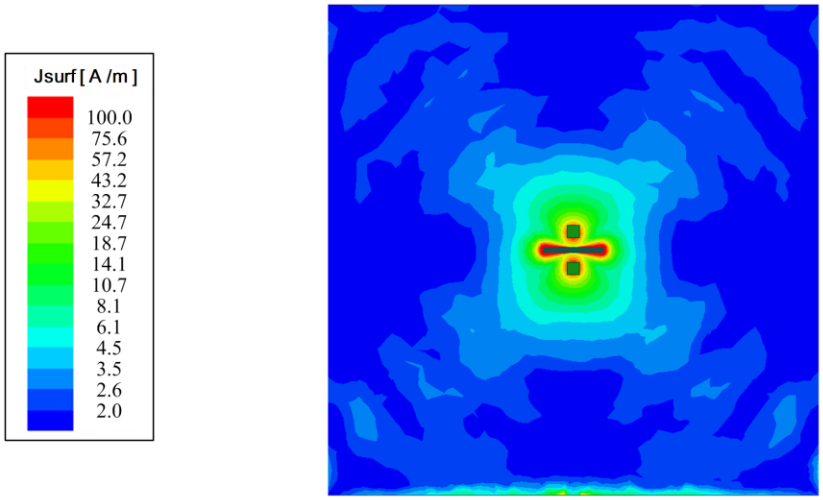

Figure 6. Currents distribution on the top layer of the SIW at 24 GHz.

Figure 7 show the simulated reflection coefficient of the dielectric rod antenna. A good impedance match is observed in the upper frequency band. The −10 dB bandwidth is 1.6 GHz (23.8–25.4 GHz), which is sufficient to cover the 24–24.25 GHz ISM band.

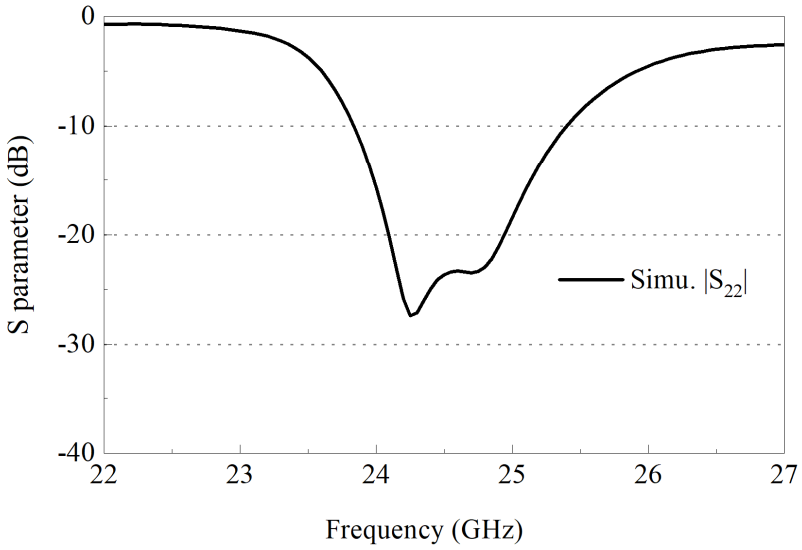

Figure 7. Simulated reflection coefficient of the dielectric rod antenna.

The influence of the ground plane is investigated. Figure 8 show the simulated radiation patterns with different sizes of ground plane. It is seen that the radiation patterns in the two principal planes remain stable, although the size of the ground plane changes a lot. The size variation of the ground plane has little influence on the dielectric rod antenna. This property is useful when integrating the dielectric rod with the patch array since the ground plane of the patch array is large.

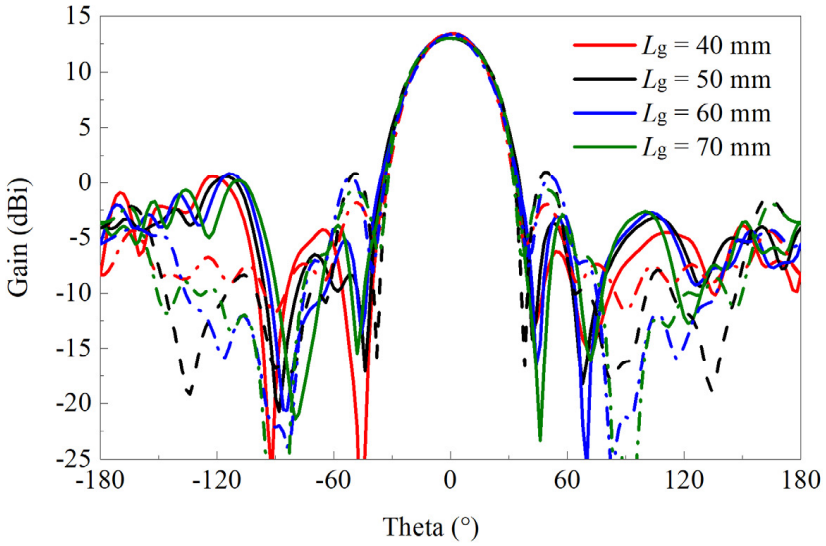

Figure 8. The influence of the ground plane on the radiation patterns. The solid and dashed lines refer to *x*-*z* and *y*-*z* planes, respectively.

Considering that the patch array and the dielectric rod for the lower and upper bands have no overlapping radiating aperture, the two radiators can work independently. High port isolation is obtained in the two bands. Equal beamwidth can be achieved by separately tuning the length of the dielectric rod antenna.

2.3. Operating Principle of the 2 × 2 Patch Array

Patch array is used to generate a pencil beam in the lower band. It should be pointed out that a patch array is just the typical example; other kinds of antennas can also be used. The 2 × 2 patch array is fed by a four-way power divider. Considering that the elements are fed from the top and bottom sides, a 180° phase shifter is used to make sure that all the elements are excited in phase. The upper substrate layer for the ME dipole design is also utilized for patch design. Therefore, no additional substrate is needed for the lower band design. The RT/duroid 5880 substrate (ε_r = 2.2, tan δ = 0.0009) has a thickness of 1.575 mm. The size of the ground plane is 70 × 70 mm^2. Port 1 is connected with an SMA connector from the bottom of the antenna.

The center frequency of the patch array is designated at 5.8 GHz. Figure 9 shows the instantaneous current distribution on the patch array and the feed network. It is clearly observed that the feed network can provide four ways of signals with in-phase or out-of-phase excitations. The currents on the four patches are almost the same, which imply that the phase gradient of the patch array is zero. Therefore, a broadside radiation pattern will be generated.

The simulated radiation patterns of the patch array are shown in Figure 10. It is observed that the peak gain is 12.7 dBi. The 3-dB beamwidth in the *x*-*z* and *y*-*z* planes is 40° and 43.6°, respectively. The two values are close, which means that the pencil beam is generated in the lower frequency band.

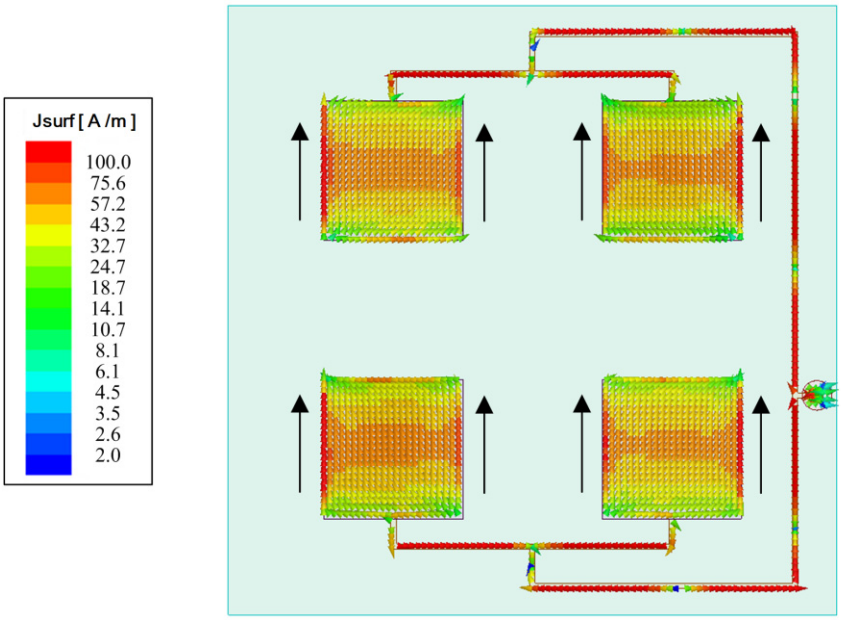

Figure 9. Currents distribution on the patch array at 5.8 GHz.

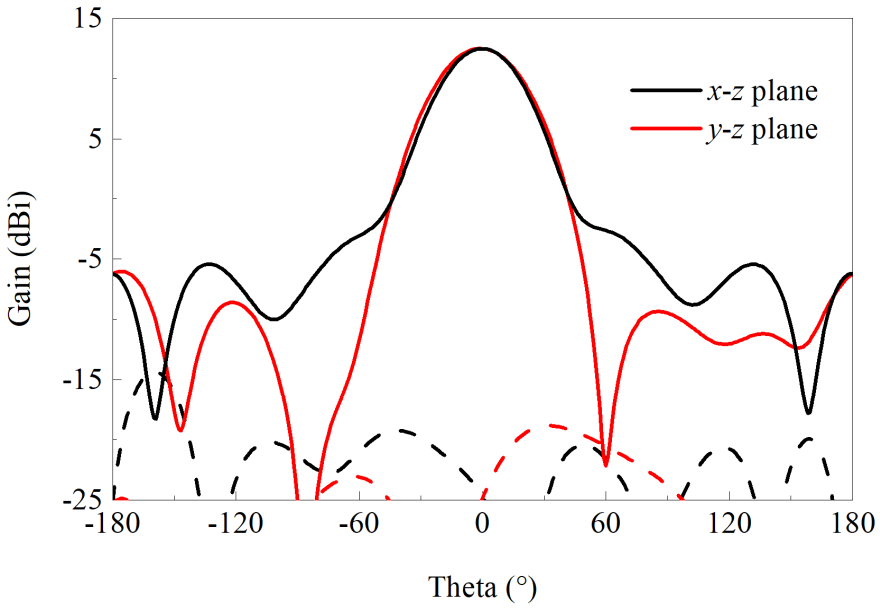

Figure 10. Simulated radiation patterns of the patch array at 5.8 GHz. The solid and dashed lines refer to the co- and cross-polarizations, respectively.

3. Experimental Results

A prototype of the hybrid antenna is fabricated and measured. Figure 11 shows the photograph of the assembled antenna. The dielectric rod is glued at the center of the substrate board. The two substrate layers of the SIW feeder are assembled using plastic screws. A metallic ring with shorting pins is added on the upper substrate, which surrounds the dielectric rod. It is useful to align the rod with the substrate. The introduction of the glue and ring has little influence on the performance via simulation verification. An SMA connector and a K connector are soldered for the lower and upper bands, respectively. It should be mentioned that the mechanical stability of the structure can be strengthened by adding stubs at the bottom of the rod, which is used to fasten the rod on the substrate with plastic screws.

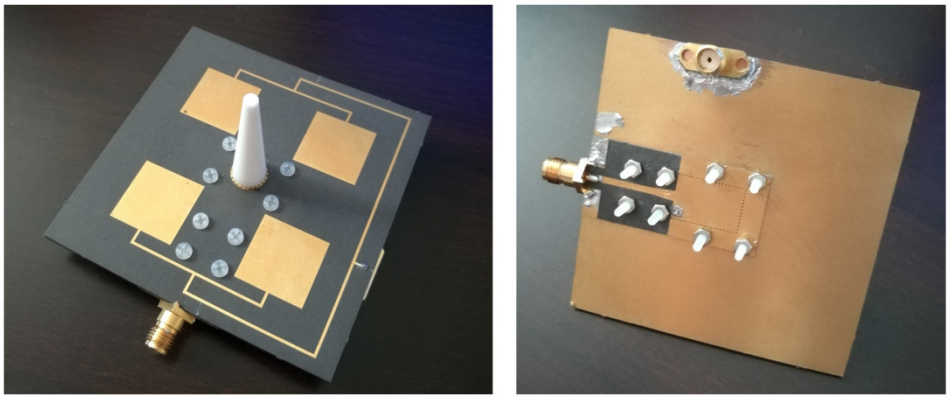

Figure 11. Photograph of the fabricated antenna. Left side is the top view and right side is the bottom view.

Figures 12 and 13 show the S parameters in the lower and upper bands, respectively. The simulated and measured curves of $|S_{11}|$ agree well in the lower band. The measured −10 dB bandwidth is 350 MHz (5.67–6.02 GHz), which is sufficient to cover the 5.725–5.875 GHz ISM band. The measured port isolation ishigher than −40 dB. In the upper band, the measured $|S_{22}|$ has some frequency shift from the simulated one. This difference may be attributed to fabrication errors. The measured −10 dB bandwidth is roughly 1.8 GHz, ranging from 23.4 GHz to 25.2 GHz, which can cover the 24–24.25 GHz ISM band. The measured port isolation is higher than 30 dB.

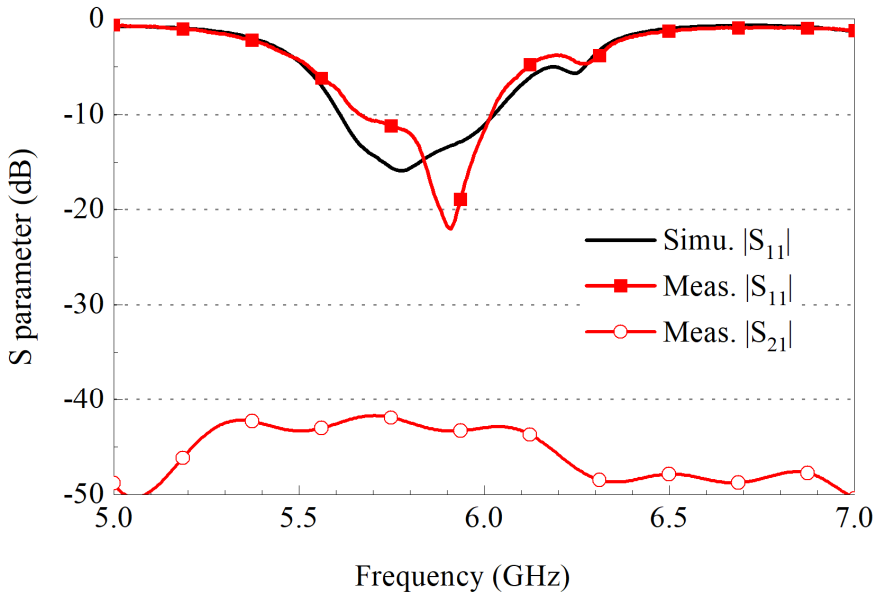

Figure 12. Simulated and measured S parameters in the lower frequency band.

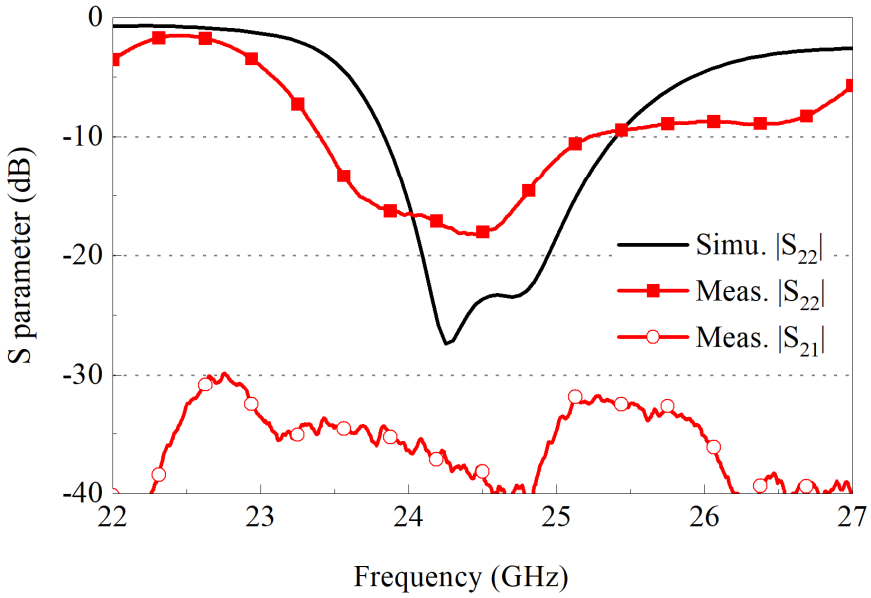

Figure 13. Simulated and measured S parameters in the upper frequency band.

The radiation patterns at the two bands are measured in a far-field chamber. During the measurement, when one feed port is excited, the other feed port is terminated with a 50 Ω load. A total of 5.8 GHz and 24 GHz are selected to represent the typical frequency points in the lower and upper bands. Figures 14 and 15 show the simulated and measured normalized radiation patterns at the two frequencies. The simulated and measured curves show reasonable agreements. Pencil beams can be observed at both 5.8 GHz and 24 GHz. At 5.8 GHz, the measured 3-dB beamwidth in the *x*-*z* and *y*-*z* planes is 42° and 43°. At 24 GHz, the 3-dB beamwidth in the two planes is 39° and 42°. These values are close. Therefore, almost equal 3-dB beamwidth is achieved in the two frequency bands. The cross-polarization levels are all below −18 dB in the two principal planes. The measured peak gain at 5.8 GHz and 24 GHz is 12.5 dBi and 12.7 dBi.

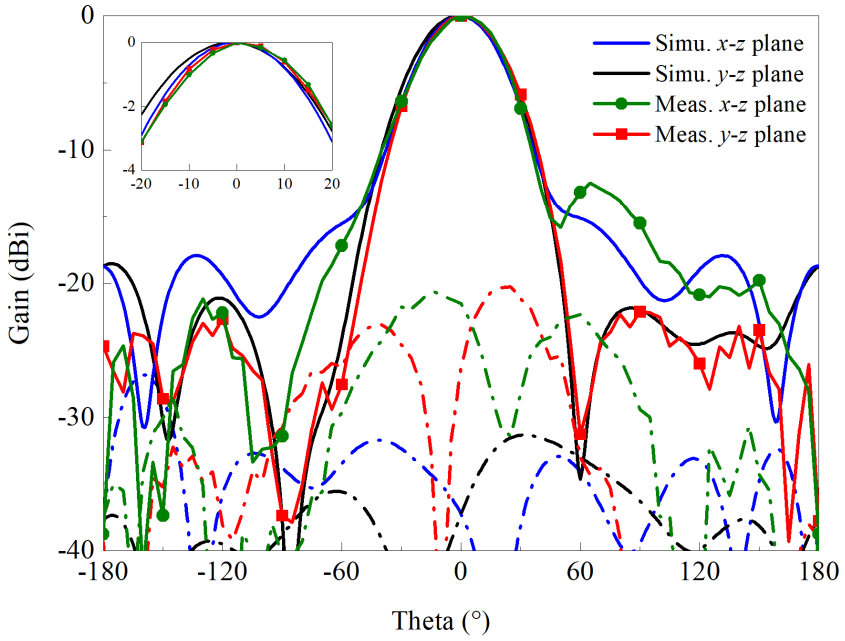

Figure 14. Simulated and measured normalized radiation patterns at 5.8 GHz.

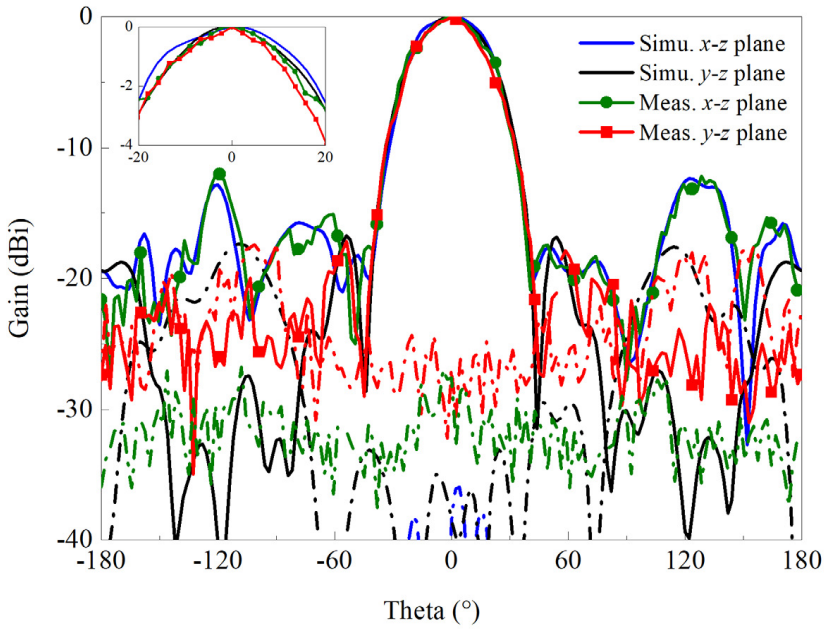

Figure 15. Simulated and measured normalized radiation patterns at 24 GHz.

4. Discussion

The performances of the proposed design and other referenced dual-band antennas are compared. As shown in Table 2, the proposed design has the advantages of equal beamwidth and equal gain in two frequency bands. To the best of the authors' knowledge, this is the first time that the issue of identical illumination in two bands has beentackled. In the future, research will be focused on other combinations of radiators and designing a high gain dual-band antenna with equal beamwidth.

Table 2. Comparisons of the proposed antenna with other dual-band antenna.

Design	f_1(GHz)	f_2 (GHz)	Beamwidth at f_1 (°)	Beamwidth at f_2 (°)	Gains at f_1 and f_2 (dBi)
[11]	12.45	14.35	~13/not given	~11/not given	~22/23
[14]	12.1	17.4	19.1/not given	13.1/not given	18/18.2
[15]	7.28	8	~22/not given	~16/not given	12.98/13.25
[18]	1.275	1.575	~82/88	~74/76	8.2/8.7
[22]	5.8	30	22/34	56/68	10.2/8.1
Proposed	5.8	24	42/43	39/42	12.5/12.7

5. Conclusions

The concept of realizing equal beamwidth in two frequency bands is presented for the first time. As a proof of concept, a 2 × 2 patch array and a dielectric rod antenna are integrated to provide dual-band operation. The beamwidth of the rod is adjusted to coincide with that of the patch array. The dielectric rod is fed by a planar SIW rather than a bulky 3-D waveguide. A novel ME dipole is constructed to amend the radiation distortion caused by the planar SIW feeder. The measured reflection coefficient bandwidth is 0.35 GHz in the 5.8 GHz band and 1.8 GHz in the 24 GHz band, with port isolation higher than 30 dB. The measured 3-dB beamwidth is around 40° in the two bands. The equal beamwidth illumination property is attractive in dual-band radar. The proposed dual-band antenna will be applied in cloud radar that uses two independent frequency channels to detect cloud particles.

Author Contributions: Conceptualization, N.Z.; methodology, N.Z.; software, N.Z.; validation, N.Z.; formal analysis, C.D.; investigation, C.D.; resources, C.D.; data curation, C.D.; writing—original draft preparation, C.D.; writing—review and editing, H.S.; visualization, C.D.; supervision, H.S.; project administration, H.S.; funding acquisition, H.S. All authors have read and agreed to the published version of the manuscript.

Funding: This research was funded by the National Natural Science Foundation of China under Contract 62071037.

Data Availability Statement: All data are included within manuscript.

Conflicts of Interest: The authors declare no conflict of interest.

References

1. Scotti, F.; Laghezza, F.; Onori, D.; Bogoni, A. Field trial of a photonics-based dual-band fully coherent radar system in a maritime scenario. *IET Radar Sonar Navig.* **2016**, *11*, 420–425. [CrossRef]
2. Nouguier, F.; Mouche, A.; Rascle, N.; Chapron, B.; Vandemark, D. Analysis of dual-frequency ocean backscatter measurements at Ku- and Ka-bands using near-nadir incidence GPM radar data. *IEEE Geosci. Remote Sens. Lett.* **2016**, *13*, 1310–1314. [CrossRef]
3. Jain, V.; Sundararaman, S.; Heydari, P. A single-chip dual-band 22–29-GHz/77–81-GHz BiCMOS transceiver for automotive radars. *IEEE J. Solid-State Circuits* **2009**, *44*, 3469–3485. [CrossRef]
4. Schmalz, K.; Rothbart, N.; Gluck, A.; Eissa, M.H.; Mausolf, T.; Turkmen, E.; Yilmaz, S.B.; Hübers, H.-W. Dual-band transmitter and receiver with bowtie-antenna in 0.13 µm SiGeBiCMOS for gas spectroscopy at 222–270 GHz. *IEEE Access* **2021**, *9*, 12485–124816. [CrossRef]
5. Maleki, A.; Oskouei, H.D.; MohammadiShirkolaei, M. Miniaturized microstrip patch antenna with high inter-port isolation for full duplex communication system. *Int. J. RF MicrowComput. Aided Eng.* **2021**, *31*, e22760. [CrossRef]
6. Althuwayb, A.A. Enhanced radiation gain and efficiency of a metamaterial inspired wideband microstrip antenna using substrate integrated waveguide technology for sub-6 GHz wireless communication systems. *Microw. Opt. Technol. Lett.* **2021**, *63*, 1892–1898. [CrossRef]
7. Mohammad, A.K.; Mohammad, N.M.; Ramazan, A.S. Composite right–left-handed-based antenna with wide applications in very-high frequency–ultra-high frequency bands for radio transceivers. *IET Microw. Antennas Propag.* **2015**, *9*, 1713–1726.
8. Wang, J.; Ge, J.; Zhou, Y.; Xia, H.; Yang, X. Design of a high- isolation 35/94-GHz dual-frequency orthogonal-polarization Cassegrain antenna. *IEEE Antennas Wirel. Propag.* **2017**, *16*, 1297–1300. [CrossRef]
9. Malfajani, R.S.; Arand, B.A. Dual-band orthogonally polarized single-layer reflectarray antenna. *IEEE Trans. Antennas Propag.* **2017**, *65*, 6145–6150. [CrossRef]
10. Martinez-de-Rioja, E.; Martinez-de-Rioja, D.; López-Sáez, R.; Linares, I. High-efficiency polarizer reflectarray antennas for data transmission links from a cubeSat. *Electronics* **2021**, *10*, 1802. [CrossRef]
11. Ma, X.; Huang, C.; Pan, W.; Zhao, B.; Cui, J.; Luo, X. A dual circularly polarized horn antenna in Ku-band based on chiral metamaterial. *IEEE Trans. Antennas Propag.* **2014**, *62*, 2307–2311. [CrossRef]
12. Ando, T.; Ohba, I.; Numata, S.; Yamauchi, J.; Nakano, H. Linearly and curvilinearly tapered cylindrical-dielectric-rod antennas. *IEEE Trans. Antennas Propag.* **2005**, *53*, 2827–2833. [CrossRef]
13. Nasir, M.; Xia, Y.; Jiang, M.; Zhu, Q. A novel integrated Yagi–Uda and dielectric rod antenna with low sidelobe level. *IEEE Trans. Antennas. Propag.* **2019**, *67*, 2751–2756. [CrossRef]
14. Zhang, J.D.; Wu, W.; Fang, D.G. Dual-band and dual-circularly polarized shared-aperture array antennas with single-layer substrate. *IEEE Trans. Antennas Propag.* **2016**, *64*, 109–116. [CrossRef]
15. Chen, C.; Liu, Z.; Wang, H.; Guo, Y. Metamaterial-inspired self polarizing dual band dual-orthogonal circularly polarized Fabry-Perot resonator antennas. *IEEE Trans. Antennas Propag.* **2019**, *67*, 1329–1334. [CrossRef]
16. Catalani, A.; Toso, G.; Angeletti, P.; Albertini, M. Development of enabling technologies for Ku-band airborne SATCOM phased-arrays. *Electronics* **2020**, *9*, 488. [CrossRef]
17. Wang, Z.; Huang, Z. A microwave/millimeter wave dual-band shared aperture patch antenna array. *IEEE Access* **2020**, *8*, 218585–218591. [CrossRef]
18. Pelliccia, E.; VincentiGatti, R.V.; Angeletti, P.; Toso, G. A dual-band circularly polarized patch array antenna for phase-only beam shaping with element rotation. *Electronics* **2021**, *10*, 643. [CrossRef]
19. Kothapudi, V.K.; Kumar, V. A multi-layer S/X-band shared aperture antenna array for airborne synthetic aperture radar applications. *Int. J. RF Microw. Comput. Aided Eng.* **2021**, *31*, e22720. [CrossRef]
20. Li, Y.; Zhang, Z.; Zheng, J.; Feng, Z.; Iskander, M.F. A compact hepta-band loop-inverted F reconfigurable antenna for mobile phone. *IEEE Trans. Antennas Propag.* **2012**, *60*, 389–392. [CrossRef]
21. Deng, C.; Li, Y.; Zhang, Z.; Pan, G.; Feng, Z. Dual-band circularly polarized rotated patch antenna with a parasitic circular patch loading. *IEEE Antennas Wirel. Propag. Lett.* **2013**, *12*, 492–495. [CrossRef]
22. Xiang, B.J.; Zheng, S.Y.; Wong, H.; Pan, Y.M.; Wang, K.X.; Xia, M.H. A flexible dual-band antenna with large frequency ratio and different radiation properties over the two bands. *IEEE Trans. Antennas Propag.* **2018**, *66*, 657–667. [CrossRef]

23. Tang, M.; Wu, Z.; Shi, T.; Ziolkowski, R.W. Dual-band, linearly polarized, electrically small huygens dipole antennas. *IEEE Trans. Antennas Propag.* **2019**, *67*, 37–47. [CrossRef]
24. Chung, M.-A.; Yang, C.-W. Miniaturized broadband-multiband planar monopole antenna in autonomous vehicles communication system device. *Electronics* **2021**, *10*, 2715. [CrossRef]
25. Li, X.-P.; Xu, G.; Ma, M.-R.; Duan, C.-J. UWB dual-band-notched lanky-leaf-shaped antenna with loaded half-square-like slots for communication system. *Electronics* **2021**, *10*, 1991. [CrossRef]
26. Raheel, K.; Altaf, A.; Waheed, A.; Kiani, S.H. E-shaped H-slotted dual band mmWave antenna for 5G technology. *Electronics* **2021**, *10*, 1019. [CrossRef]
27. Huang, J.; Dong, G.; Cai, J.; Li, H. A quad-port dual-band MIMO antenna array for 5G smartphone applications. *Electronics* **2021**, *10*, 542. [CrossRef]
28. Ji, Z.; Wang, K.X.; Wong, H. Circularly polarized dielectric rod waveguide antenna for millimeter-wave applications. *IEEE Trans. Antennas Propag.* **2018**, *66*, 5080–5087. [CrossRef]
29. Zhang, Y.; Lin, S.; Zhu, B.; Cui, J.; Denisov, A. Broadband and high gain dielectric-rod endfire antenna fed by a tapered ridge waveguide for K/Ka bands applications. *IET Microw. Antennas Propag.* **2020**, *14*, 743–751. [CrossRef]
30. Sporer, M.; Weigel, R.; Koelpin, A. A 24 GHz dual-polarized and robust dielectric rod Antenna. *IEEE Trans. AntennasPropag.* **2017**, *65*, 6952–6959. [CrossRef]
31. Kazemi, R.; Fathy, A.E.; Sadeghzadeh, R.A. Dielectric rod antenna array with substrate integrated waveguide planar feed network for wideband applications. *IEEE Trans. Antennas Propag.* **2012**, *60*, 1312–1319. [CrossRef]
32. Ghassemi, N.; Wu, K. Planar dielectric rod antenna for gigabyte chip-to-chip communication. *IEEE Trans. Antennas Propag.* **2012**, *60*, 4924–4928. [CrossRef]
33. Leib, M.; Vollmer, A.; Menzel, W. An ultra-wideband dielectric rod antenna fed by a planar circular slot. *IEEE Trans. Microw. Theory Techn.* **2011**, *59*, 1082–1089. [CrossRef]
34. Patrovsky, A.; Wu, K. 94-GHz planar dielectric rod antenna with substrate integrated image guide (SIIG) feeding. *IEEE Antennas Wirel. Propag. Lett.* **2006**, *5*, 435–437. [CrossRef]
35. Althuwayb, A.A. Low-interacted multiple antenna systems based on metasurface-inspired isolation approach for MIMO applications. *Arab. J. Sci. Eng.* **2021**, e05720. [CrossRef]
36. Mohammad, A.; Virdee, B.S.; Azpilicueta, L.; Naser-Moghadasi, M.; Akinsolu, M.O.; See, C.H.; Liu, B.; Abd-Alhameed, R.A.; Falcone, F.; Huynen, I.; et al. A comprehensive survey of "metamaterial transmission-line based antennas: Design, challenges, and applications. *IEEE Access.* **2020**, *8*, 144778–144808.
37. Mohammadi, S.M. Wideband linear microstrip array antenna with high efficiency and low side lobe level. *Int. J. RF Microw. Comput. Aided. Eng.* **2020**, *30*, e22412.
38. Wu, Q.; Luk, K.M. A broadband dual-polarized magneto-electric dipole antenna with simple feeds. *IEEE Antennas Wirel. Propag. Lett.* **2009**, *8*, 60–63.